

---

# EEG-LANGUAGE MODELING FOR PATHOLOGY DETECTION

---

A PREPRINT

**Sam Gijzen, Kerstin Ritter**

Charité – Universitätsmedizin Berlin, Department of Psychiatry and Psychotherapy, Berlin, Germany  
Hertie Institute for AI in Brain Health, University of Tübingen, Germany  
sam.gijzen@charite.de, kerstin.ritter@charite.de

## ABSTRACT

Multimodal language modeling constitutes a recent breakthrough which leverages advances in large language models to pretrain capable multimodal models. The integration of natural language during pretraining has been shown to significantly improve learned representations, particularly in computer vision. However, the efficacy of multimodal language modeling in the realm of functional brain data, specifically for advancing pathology detection, remains unexplored. This study pioneers EEG-language models trained on clinical reports and 15000 EEGs. We extend methods for multimodal alignment to this novel domain and investigate which textual information in reports is useful for training EEG-language models. Our results indicate that models learn richer representations from being exposed to a variety of report segments, including the patient’s clinical history, description of the EEG, and the physician’s interpretation. Compared to models exposed to narrower clinical text information, we find such models to retrieve EEGs based on clinical reports (and vice versa) with substantially higher accuracy. Yet, this is only observed when using a contrastive learning approach. Particularly in regimes with few annotations, we observe that representations of EEG-language models can significantly improve pathology detection compared to those of EEG-only models, as demonstrated by both zero-shot classification and linear probes. In sum, these results highlight the potential of integrating brain activity data with clinical text, suggesting that EEG-language models represent significant progress for clinical applications.

## 1 Introduction

Medical neuroimaging such as electroencephalography (EEG) has not yet benefited to the same extent as other domains from the considerable advances deep learning has brought about. While EEG sees widespread clinical use for pathology detection, in particular for epilepsy [1, 2] as well as sleep disorders [3], available annotated data is scarce. As the impressive scaling properties of deep learning are now well described [4, 5], self-supervised learning (SSL) is a promising direction by enabling pretraining with unlabeled data and thereby increasing available training sample sizes [6, 7]. Various such approaches have shown initial success when applied to EEG. These include methods relying on data-augmentations [8, 9], the temporal ordering of EEG data [10], as well as masking and reconstruction [11]. However, these are hindered by the difficulty of creating appropriate data augmentations and, especially reconstruction techniques, by low signal-to-noise. Thus, progress in the medical context has lagged, likely further exacerbated by the modality displaying high similarity between pathologies.

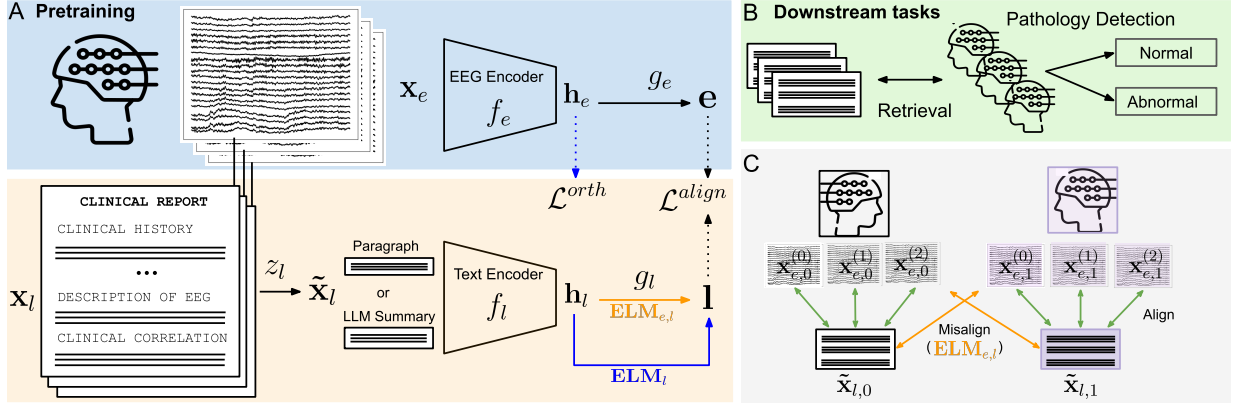


Figure 1: Overview of the methodology. **A)** The EEG and text encoding pathways are displayed. Arrows in orange (blue) denote operations only used by  $ELM_{e,l}$  ( $ELM_l$ ).  $h_e$  and  $e$ : EEG embedding prior and post projection,  $h_l$  and  $l$ : text embedding prior and post projection **B)** Summary of the downstream tasks of EEG or clinical report retrieval and pathology detection. **C)** Visualization of the current extension of multimodal language modeling to EEG timeseries, which are cut into sequential crops.

Meanwhile, important further progress was made in computer vision by leveraging natural language as a signal during pretraining [12]. Specifically, contrastive approaches which aim to align embeddings of image-text pairs have shown to yield representations powerful for downstream tasks in radiology [13, 14]. Given that success in radiology is also believed to be bottlenecked by the availability of labeled data and the reliance on fine-grained information [13], this joint modeling approach is a particularly interesting and novel application for the challenging problem of medical EEG. Fortunately, this is made possible by the clinical reports of physicians which accompany hospital EEG recordings and contain information about the patient and recording itself [15].

However, language-EEG pretraining also entails unique challenges. First, datasets are generally smaller than those used in radiology. As a consequence, models used for EEG tend to be smaller, which, when jointly trained with a much larger language model, may lead to unstable training and dimensional collapse of the latent space [16, 17]. Second, the clinical reports tend to be highly heterogeneous in both content and length. While previous applications have paired natural and medical images with short captions [12, 13], EEG reports tend to span multiple paragraphs and include information irrelevant to downstream clinical tasks, potentially hindering the pretraining process.

The current work investigates the application of aligning functional brain data with medical textual information for the first time. To address challenges associated with data scarcity, we integrate recent methodological developments in multimodal pretraining for medical imaging to regularize the latent space [17] and compare these to a contrastive learning approach. Furthermore, we investigate how to best handle the heterogeneity of medical EEG reports. Specifically, we perform content-based text segmentation, enabling inference on the relative importance of the different sources of information in the reports, such as clinical history, medication, description of the recording, and the physician’s impression. These approaches are additionally compared to the use of a large generative language model to summarize clinical reports, which may be steered for specific downstream tasks. To study the information learned by EEG-language models, we perform retrieval analyses of clinical reports or EEG. We furthermore test downstream performance on classifying normal and pathologically abnormal EEG, which is a widespread clinical task. These tests include zero-shot classification by leveraging the language capabilities to evaluate the flexibility of the approach. Consequently, we provide insight into the novel extension of current multimodal language modeling to the domain of medical brain activity. Our results constitute considerable increases in pathology detection performance in scenarios with few labels. These are particularly relevant for clinical contexts, which tend to operate with smaller datasets compared to many common areas of deep learning applications.

## 2 Related work

- **Self-supervised learning with EEG data.** SSL with EEG data has been predominantly applied to emotion recognition [18, 19], motor imagery [20, 21], sleep staging [9, 21], as well as pathology detection. For the latter application, the temporal order of EEG crops was used initially to demonstrate label-efficient representation learning [10]. Contrastive learning, combined with larger EEG encoders trained on multiple datasets, further improved pathology detection [8]. In this case, the model was trained for invariance to a set of data augmentations, based on the SimCLR work in computer vision [7]. Whereas most work uses convolutional and recurrent architectures, recent studies have explored

transformers [22, 11]. These have focused on scaling and adopted tokenization in an attempt to improve the challenge of effective cross-dataset EEG training. They rely on masking and reconstruction pretext tasks.

- **Using EEG for pathology detection.** While SSL shows good performance for pathology detection, it is particularly in contexts with little annotated data that it performs well. When more labeled data is available, expert-based feature extraction combined with traditional machine learning classifiers are competitive together with supervised deep learning [23, 24, 25, 26, 27]. The observation of similar classification performance between deep learning and feature-based approaches has also been made for other EEG applications [28, 29]. As a consequence, it has been posited that label noise could induce a ceiling effect on classification performance [30, 24]; specifically, the inter-rater reliability of EEG classification into normal or pathologically abnormal by neurologists. Although still only a hypothesis, if this is so, a focus on improving low-label classification performance may be of extra importance.
- **Medical multimodal language modeling.** Medical vision-language modeling aims to guide self-supervised pre-training on medical images using textual information in reports, with performance on a variety of downstream tasks benefiting as a result [31, 32, 13]. Recent results indicated that the finetuning of large language encoders is not necessary [17]. Due to less available data in the medical domain, using a pretrained encoder and freezing its weights considerably reduces computational cost while boosting downstream performance [17]. This was attributed to avoiding collapse in latent space by directly aligning image embeddings to the frozen text embeddings and additional regularization. Nevertheless, this line of work focuses mainly on the X-ray, CT images, and structural MRI images [33, 34]. Recently, multimodal language modeling has been performed using electrocardiogram data for cardiac pathology detection. Besides confirming the good performance using frozen language models, this work suggests effectiveness of combining functional timeseries data with textual information in a medical context [35, 36, 37, 38].

## 3 Methods

### 3.1 Experimental Setup

#### 3.1.1 EEG-language pretraining

Here we detail the setup for pretraining EEG-language models (ELMs). Whereas vision-language models are typically trained by aligning a 2D image with a short caption [13, 12], EEG-language modeling is confronted with long EEG time series and multi-paragraph medical reports. To overcome this, we employ text segmentation and time series cropping to create multiple non-overlapping samples per modality and subject. Next, we propose sub-unit alignment by pretraining on these cropped samples. In addition to considerably increasing sample size, this enables the extension of successful approaches in vision-language models. Specifically, we compare two strategies in combination with sub-unit alignment. First, EEG and text representations may be projected using neural networks to a new, shared latent space prior to alignment (as in CLIP; [13, 12]), denoted henceforth as  $\text{ELM}_{e,l}$ . Alternatively, the EEG embeddings may be projected into the output space of the language model (as in M-FLAG by [17]), denoted as  $\text{ELM}_l$ .

For EEG-language pretraining we assume the paired input  $(\mathbf{x}_{e,i}, \mathbf{x}_{l,i})$ . Here  $\mathbf{x}_{e,i} \in \mathbb{R}^{c \times s}$  denotes one or a batch of crops of EEG signal with  $c$  channels and  $s$  time samples belonging to EEG recording  $i$ . Meanwhile, neural signals of recording  $i$  as well as patient information is described in  $\mathbf{x}_{l,i}$ , which represents a natural language text report. The main goal is to train the EEG encoder function  $f_e$ , which projects a crop of EEG signal into a vector of lower dimensionality. Following pretraining, this encoder function  $f_e$  can be used for downstream applications such as pathology detection.

Dropping the recording subscript  $i$  for brevity, each pair  $(\mathbf{x}_e, \mathbf{x}_l)$  is projected into the vectors  $\mathbf{e} \in \mathbb{R}^d$  and  $\mathbf{l} \in \mathbb{R}^d$  respectively. For every  $\mathbf{x}_e$ , text of the associated report is sampled according to  $\tilde{\mathbf{x}}_l = z_l(\mathbf{x}_l)$ , where  $z_l$  represents the language sampling function detailed below. First, both the EEG crop  $\mathbf{x}_e$  and text  $\tilde{\mathbf{x}}_l$  are encoded into vectors  $\mathbf{h}_e$  and  $\mathbf{h}_l$ . For  $\text{ELM}_{e,l}$ , we use projectors  $g_e$  and  $g_l$  to yield vectors  $\mathbf{e}$  and  $\mathbf{l}$ , whereas for  $\text{ELM}_l$  the text embedding are not projected:

$$\mathbf{e} = g_e(f_e(\mathbf{x}_e)) \quad (1)$$

$$\mathbf{l} = \begin{cases} g_l(f_l(\tilde{\mathbf{x}}_l)) & \text{if } \text{ELM}_{e,l} \\ f_l(\tilde{\mathbf{x}}_l) & \text{if } \text{ELM}_l \end{cases} \quad (2)$$

To enable multimodal pretraining, the projectors  $g_e$  and  $g_l$  map  $\mathbf{e}$  and  $\mathbf{l}$  to a shared latent space with identical dimensionality  $d$ . For  $\text{ELM}_l$ , this is achieved by having  $g_e$  project to the native dimensionality of the text encoder  $f_l$ .

As paired medical EEG data and clinical reports are scarce, training the text encoder function  $f_l$  from scratch is unlikely to be successful. Furthermore, employing an existing language model and finetuning the model during multimodal pretraining can lead to training instability and collapse of the latent space [16, 17]. To prevent resulting information

loss, we follow the recommendations by Liu et al. [17] to use a pretrained language model for  $f_l$  and freeze its weights during training. We adopt their proposed composite loss for  $\text{ELM}_l$  to learn  $f_e$  and  $g_e$ :

$$\mathcal{L}_{total} = \mathcal{L}_{align} + \mathcal{L}_{orth} \quad (3)$$

$$\mathcal{L}_{align} = \|\mathbf{e} - \mathbf{1}\|_2^2 = 2 - 2\mathbf{e}^\top \mathbf{1} \quad (4)$$

$$\mathcal{L}_{orth} = \sum_{j=1} \left(1 - (\mathbf{h}_e^\top \cdot \mathbf{h}_e)_{jj}\right)^2 + \sum_{j \neq k} (\mathbf{h}_e^\top \cdot \mathbf{h}_e)_{jk}^2, \quad (5)$$

where  $\{j, k\} \in \{1, \dots, \dim(\mathbf{h}_e)\}^2$  and  $\mathbf{h}_e$  denotes a batch of EEG embeddings. Whereas  $\mathcal{L}_{align}$  minimizes the difference between  $\mathbf{e}$  and  $\mathbf{1}$ ,  $\mathcal{L}_{orth}$  promotes independence between latent dimensions of  $\mathbf{h}_e$ . More specifically, the latter is achieved by manipulating the empirical correlation matrix, where the diagonal and off-diagonal elements are pushed to 1 and 0 respectively [17].

Meanwhile,  $\text{ELM}_{e,l}$  relies on the cosine similarities between normalized EEG and text embeddings,  $s_{j,j}^{e2l} = \hat{\mathbf{e}}_j^\top \hat{\mathbf{l}}_j$ , and between text and EEG,  $s_{j,j}^{l2e} = \hat{\mathbf{l}}_j^\top \hat{\mathbf{e}}_j$ , with  $j = 1, 2, 3, \dots, N$  for batch size  $N$  [12]. The multimodal contrastive loss uses a temperature hyperparameter  $\tau$  (set to 0.3; Appendix A.4) and is formulated as:

$$\mathcal{L}_{j,k}^{e2l} = -\log \frac{\exp(s_{j,k}^{e2l}/\tau)}{\sum_{m=1}^N \exp(s_{j,m}^{e2l}/\tau)} \quad (6)$$

$$\mathcal{L}_{j,k}^{l2e} = -\log \frac{\exp(s_{j,k}^{l2e}/\tau)}{\sum_{m=1}^N \exp(s_{j,m}^{l2e}/\tau)} \quad (7)$$

$$\mathcal{L}_{align} = \frac{1}{2N} \sum_{j=1}^N \sum_{k=1}^N (\mathcal{L}_{j,k}^{e2l} + \mathcal{L}_{j,k}^{l2e}) \quad (8)$$

**Language encoder.** For  $f_l$  we use a transformer model which was pretrained in a contrastive manner on PubMed search logs (MedCPT [39]), which is based on PubMedBERT [40]. See Appendix A.3 for a comparison of language models.  $\text{ELM}_l$  adopts the language model’s native hidden dimensionality (768), while for  $\text{ELM}_{e,l}$  we project to a dimensionality of 256.

**EEG encoder.** For the EEG encoder  $f_e$  we use a randomly initialized residual convolutional neural network, with an identical architecture across the compared training contexts: self-supervised learning with only EEG data and EEG-language pretraining. We use nonlinear MLPs with a single-hidden layer for  $g_e$  and  $g_l$ , as well as for the projector head in EEG-only self-supervised learning. More details are provided in Appendix A.2.

### 3.1.2 EEG-only self-supervised learning

We compare the representations learned by EEG-language pretraining to those obtained via EEG-only pretraining. First, we employ multiple methods that train for invariance to data augmentations. This is achieved by sampling data augmentations for each EEG crop  $\mathbf{x}_e$ , resulting in two differing data views  $\{\mathbf{x}'_e, \mathbf{x}''_e\}$ . It is important the data augmentations do not destroy the semantic information in  $\mathbf{x}_e$ . Training to align the embeddings of these views while preventing collapse has been shown to yield data representations useful for downstream tasks [7, 8, 9]. We implement the following methods (Appendix A.5): Bootstrap-Your-Own-Latent (BYOL; [41]), Variance-Invariance-Covariance Regularization (VICReg; [42]), and Contrast with the World Representation (ContraWR; [9]). Additionally, we compare against methods using the temporal ordering of EEG crops: Relative Positioning (RP; [10]), Temporal Shuffling (TS; [10]), Contrastive Predictive Coding (CPC; [10]).

## 3.2 Datasets and preprocessing

- **TUEG.** The Temple University Hospital (TUH) EEG Corpus is the largest available corpus of hospital EEG data with varying montages, channel counts, and sampling frequencies ( $n=26846$  [15]). For each patient, one or more EEG sessions are provided, each of which contains one or more recordings. For most of the dataset, no labels are available beyond patient age and sex. However, each EEG session is associated with a natural-language clinical report, containing information about the patient such as demographics and clinical history, as well as the physician’s impression of EEG recording and clinical status.

- **TUAB.** The TUH Abnormal EEG corpus is a subset of TUEG which was manually labeled by clinicians indicating whether the EEG displays pathological abnormalities [43]. This enables the binary classification task of predicting the

status of {normal, abnormal}. As training (n=2717) and evaluation (n=276) sets are provided, we use the latter as a hold-out test set.

### 3.2.1 Text processing

In order to categorize the textual content in the clinical reports, we employed regular expressions matching for commonly-occurring headings (an overview is provided in Appendix E.2). These enabled the segmentation of individual reports into their respective headings with associated text paragraphs, providing insight into which information in physician reports is encoded in the EEG. We cluster headings into four categories. First, the *clinical history* cluster contains demographic information in terms of patient age and sex, as well as a brief description of relevant current and/or past pathology and symptoms. The *record description* cluster includes the physician’s observations of the EEG traces, which describes both normal and abnormal features, often in terms of oscillatory brain activity. The *medication* cluster contains the patient’s current medication information. Finally, the *interpretation* cluster summarizes a physician’s thoughts, often including the impression of whether the EEG is normal or pathologically abnormal, as well as a clinical correlation. To investigate whether EEG-language models can learn richer representations by being exposed to a larger variety of text, we also train models by sampling text from all four aforementioned clusters.

Due to the heterogeneity of the clinical reports, we further test the utility of summarizing the pathological status indicated by the clinical report using a large language model (LLM). Due to the sensitive nature of the clinical reports, we use the Llama-3 8B model [44] locally and instruct for the production of a single-sentence summary of a report, which should include whether the EEG was deemed abnormal and for which reasons (Appendix E.2).

**Language encoding.** Given a sampled paragraph from a clinical report or the LLM-generated summary, we encode this text by relying on the embedding of a special  $[cls]$  token which aggregates the representations across all tokens. As such, given a clinical report  $\mathbf{x}_l$ , the transformation function  $z_l$  corresponds to text segmentation or summarization yielding  $\tilde{\mathbf{x}}_l$ . Following tokenization, we embed into the  $[cls]$  token using  $f_l$ . The resulting text embedding  $\mathbf{h}_l$  may be used for multimodal pretraining.

### 3.2.2 EEG processing

From the EEG dataset, recordings longer than 2.5 hours were omitted to filter out a small subset of very long, potentially overnight recordings. For training efficiency, only the first 45 minutes of a recording were used. Any recording files shorter than 70 seconds were also omitted.

**EEG preprocessing.** EEG data received minimal preprocessing (using MNE [45]). First, the first 10 seconds were removed to reduce the impact of set-up artefacts. Afterwards, a bandpass filter of 0.1-49 Hz was applied and all recordings were resampled to 100 Hz. To reduce the impact of signal artefacts, all EEG signals had their amplitude clipped to  $\pm 800 \mu\text{V}$ . As a large majority of recordings used an average-reference (AR) or linked-ear reference (LE), we only used these recordings and standardized them via transformation to the 20-channel Temporal Central Parasagittal (TCP) montage. To enable fair comparisons between methods, the optimal crop-length out of  $\{5, 10, 20, 30, 60\}$  seconds was determined without data-leakage through training and evaluation on subsets of the training data only (Appendix A.2). Based on these results, we used 20 and 60 second crops for EEG-only and EEG-language modeling respectively.

### 3.2.3 Data subsampling

TUEG contains considerably more abnormal than normal EEGs. As vision-language models have been shown to be sensitive to imbalanced classes [46], we subsample the data to create approximately equal class representation. To do so, we rely on the LLM summaries of reports, which facilitated report classification based on regular expressions due to reoccurring phrasing. If any data of a subject was present in the retrieval or TUAB test set, all their data was excluded from the pretrain subset to avoid data leakage. Further details are provided in Appendix B and resulting sample sizes are shown in Table 1.

Table 1: Dataset sample sizes.

Data subset	EEG files	Clinical reports	Crops (60s)	Crops (20s)
Pretrain	15144	11785	270K	813K
TUAB train	2712	Not used	56579	170K
TUAB test	276	Not used	5783	17349
Retrieval test	437	437	8887	26661

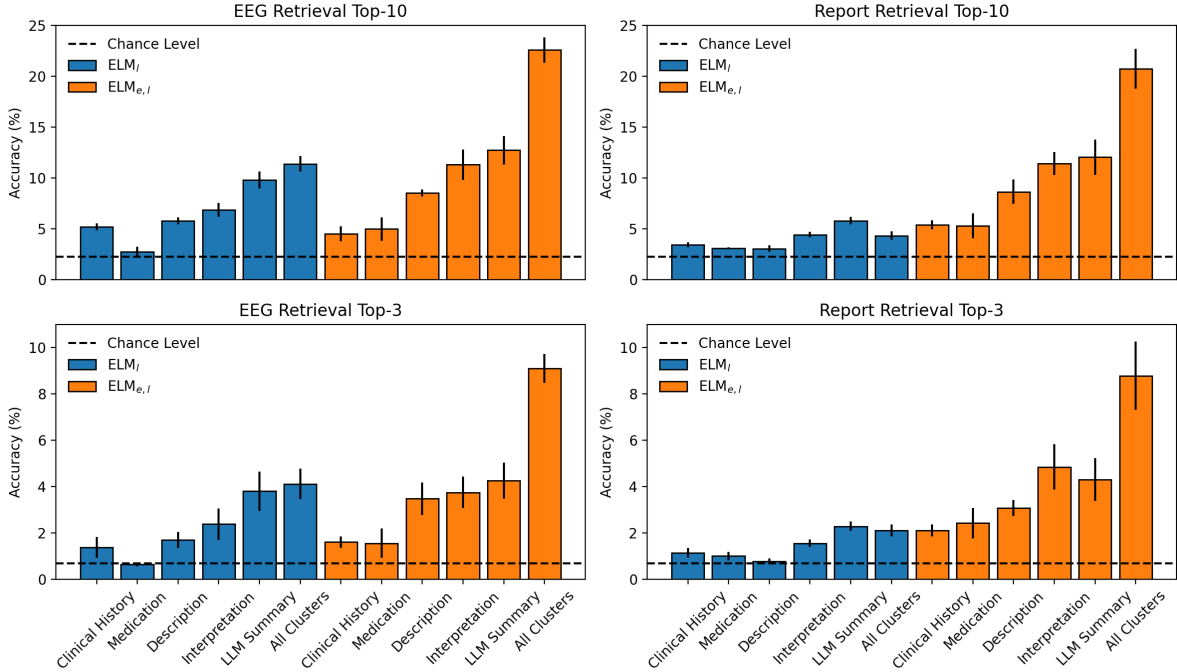


Figure 2: EEG-Language models are evaluated on their retrieval ability using top-k accuracy out of 437 patients. Either EEG is retrieved based on a queried clinical report, or vice versa. Error bars indicate standard deviations over five model training runs.

### 3.2.4 Retrieval

To investigate the information represented in the learned embeddings resulting from EEG-language training, we perform retrieval analyses. Given a medical report describing the patient and their EEG recording, we probe the ability to recover the patient’s EEG by rank-ordering candidate EEG based on embedding similarity. This analysis is also performed in opposite direction, by retrieving the associated report given an EEG recording. As reports refer to an entire recording, EEG embeddings of single crops are averaged. Given that reports generally consist of multiple paragraphs, embeddings of single paragraphs are averaged too. This procedure yields one EEG and report embedding per patient recording, which we use for rank-ordering based on cosine similarity.

The top-K retrieval accuracy, which scores whether the patient’s EEG or report has a rank equal or better than K, is plotted in Figure 2. Many models perform considerably above chance level, indicating the successful generalization of learned multimodal EEG-language information. For both EEG and report retrieval, ELM<sub>e,l</sub> models tend to outperform ELM<sub>l</sub> models. However, this discrepancy in performance is particularly prevalent for report retrieval. This is likely due to omission of a text projection head in ELM<sub>l</sub>, which may therefore lack the flexibility to appropriately separate the EEG reports in latent space. This is likely exacerbated by the current application domain: while we employ a language model finetuned for the medical domain, EEG-relevant text will only represent a small minority of the training data. Therefore, due to the similarity of the clinical reports, they may span only a relatively small part of the latent space. Meanwhile, ELM<sub>e,l</sub> performs similarly for EEG and report retrieval.

The text sampling also markedly impacts the report retrieval. The clinical history and medication clusters, which contain no direct description of the observed EEG recording, score lowest. While including such information (description cluster) helps considerably, retrieval is particularly effective when a pathology-relevant context is provided (interpretation cluster and LLM summary). This indicates that pathology is a significant source of between-subject variation. Further clear improvements are seen when text from all clusters is sampled, indicating that these clusters contain unique information and that EEG-language modeling can capture multiple dimensions of patient information.

### 3.2.5 Pathology classification

Next, we study the learned representations in their relevance to clinical pathology. To do so, we first train linear probes to detect pathology on the representations of pretrained models on TUAB under varying amounts of labels

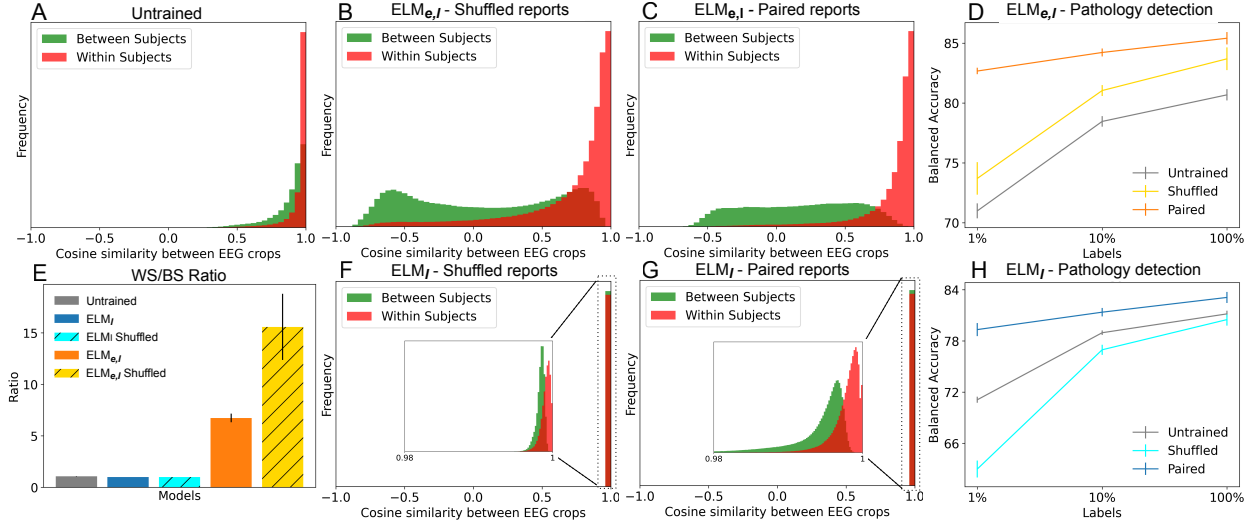


Figure 3: **A-C, E-G**) We investigate the distributions of cosine similarity values of EEG crop embeddings between- and within subjects (denoted BS and WS respectively). We plot these for an untrained encoder (one example run), as well as EEG encoders of ELMs trained with paired or shuffled reports. We find that ELM<sub>e,l</sub> produces dissimilar between-subject EEG embeddings, while ELM<sub>l</sub> does not. **E**) shows the ratio between WS and BS similarity values across five runs (with standard deviations). **D,H**) The downstream performance via linear probing is shown on the right, with error bars representing standard deviations across five training runs.

(Table 2; Appendix C). Models are trained on single EEG crops, across which we average predictions to obtain a recording-level prediction. We find EEG-language pretraining yields large improvements for pathology detection over EEG-only pretraining, with multimodal models being particularly effective at small sample sizes: at 1% of exposed labels, performance increases reach 7.7% balanced accuracy and 8.4% AUROC. In general, models with the best retrieval performance, also tend to perform better pathology detection. Nevertheless, relative performance differences between EEG-language models are smaller than for retrieval, suggesting that all models obtained representations useful for the narrower task of binary pathology detection.

**Language-independent effects of multimodal pretraining.** Given the broad outperforming of ELMs compared to EEG-only models, especially for ELM<sub>e,l</sub>, we further investigate whether the general setup of multimodal pretraining provides inherent benefits. EEG recordings are split into multiple crops, which in turn are all aligned to the same clinical report during pretraining. It follows that EEG crops of a single recording are indirectly aligned to one another to some extent (Figure 1C). We investigated this hypothesis by shuffling reports between patients prior to pretraining. We find that while embeddings of single EEG crops of an untrained encoder are only minimally more similar within-subject than between-subject (ratio of  $\sim 1.1x$ ), this effect is much more pronounced after pretraining ELM<sub>e,l</sub> on correctly paired reports ( $\sim 6.3x$ ), and even more so after pretraining on shuffled reports ( $\sim 15.7x$ ; figure 3). Linear probing reveals that training ELM<sub>e,l</sub> on shuffled reports clearly boosts pathology detection over using an untrained encoder and manages to almost match EEG-only pretraining without the need for augmentations (mean accuracies of 73.70%, 81.04%, 83.69%). On the contrary, the ratios for ELM<sub>l</sub> are close to 1 after training using paired and shuffled reports, with the latter resulting in decreased pathology detection accuracy.

Conceptually, while shuffling reports destroys the semantic relevance of reports, it still provides a unique subject-specific reference to which the EEG embeddings are aligned to. Pretraining then reduces to promoting invariance to within-subject information, as all EEG crops of a patient are aligned to the same report. However, while for ELM<sub>l</sub> these reports occupy arbitrary positions in the latent language space due to the absence of the text projector, ELM<sub>e,l</sub> exhibits additional dynamics. Namely, for a given EEG crop (or text paragraph) in a batch belonging to subject  $i$  (that is,  $id = i$ ), nearly all negative contrastive samples will belong to a different patient ( $P(id = i) \ll P(id \neq i)$ ). The negative contrast therefore largely amounts to minimizing similarity between patients. This can be viewed as encoding between-subject information and these results imply that training with this objective is a useful pretext task for EEG timeseries. Naturally, this will depend on the downstream tasks, but both retrieval and pathology detection require between-subject information. The advantage of ELM<sub>e,l</sub> and linear probing of ELM<sub>e,l</sub> may thus be, at least in part, due to the inherent utility of our extension of multimodal language modeling to timeseries by using sub-unit

alignment, independent of language. Still, pathology detection with only few annotations is considerably better using paired reports, indicating the importance of relevant clinical language for label-efficiency.

Table 2: Pathology detection via linear probing at 1%, 10%, and 100% labeled data of the TUAB training set. The best scores are printed in bold. Standard deviations over five model training runs are included.

Method	Text Sampling	Balanced Accuracy			AUROC		
		1%	10%	100%	1%	10%	100%
BYOL	-	72.69±0.57	79.03±1.16	79.94±2.14	78.85±0.81	86.75±0.76	88.82±0.70
VICReg	-	71.76±0.81	79.6±1.07	82.46±0.96	78.7±1.11	86.04±0.80	88.78±1.04
ContraWR	-	73.30±1.44	80.72±1.69	82.44±1.22	80.30±1.91	86.67±1.32	88.44±1.20
RP	-	74.52±1.06	82.16±0.38	83.36±0.42	82.63±0.87	89.78±0.43	91.43±0.34
TS	-	74.99±0.86	82.16±0.64	84.10±0.66	82.51±0.91	89.58±0.55	91.50±0.32
CPC	-	73.20±0.79	78.44±1.00	79.95±1.49	81.48±1.02	86.44±1.07	87.92±1.14
ELM <sub>l</sub>	Clinical History	76.36±0.54	79.88±1.32	82.61±1.43	84.48±1.07	87.87±1.05	89.40±0.80
ELM <sub>l</sub>	Medication	75.71±1.14	80.41±0.77	83.20±1.17	84.27±0.92	88.10±0.86	89.79±0.76
ELM <sub>l</sub>	Description	79.61±0.69	81.87±0.69	83.88±0.89	87.88±0.80	89.73±0.63	90.67±0.42
ELM <sub>l</sub>	Interpretation	80.57±0.62	81.98±1.41	83.08±1.01	88.86±0.60	89.82±0.78	90.53±0.62
ELM <sub>l</sub>	LLM Summary	82.36±0.56	83.70±0.54	84.37±0.51	90.35±0.34	90.97±0.35	91.58±0.22
ELM <sub>l</sub>	All Clusters	79.07±0.87	81.07±0.75	83.18±0.60	87.12±0.48	88.61±0.36	89.78±0.23
ELM <sub>e,l</sub>	Clinical History	79.86±0.00	82.71±0.00	84.13±0.00	87.61±0.00	90.72±0.00	91.81±0.00
ELM <sub>e,l</sub>	Medication	79.86±0.00	82.58±0.00	82.31±0.00	88.41±0.00	90.57±0.00	91.81±0.00
ELM <sub>e,l</sub>	Description	81.47±0.29	83.64±0.54	84.84±0.91	89.14±0.53	91.70±0.19	92.71±0.14
ELM <sub>e,l</sub>	Interpretation	<b>82.83</b> ±0.35	84.09±0.52	84.51±0.58	90.92±0.35	92.48±0.31	93.13±0.27
ELM <sub>e,l</sub>	LLM Summary	82.18±0.83	83.16±1.04	83.24±0.44	90.35±0.37	91.57±0.53	92.27±0.42
ELM <sub>e,l</sub>	All Clusters	82.64±0.24	<b>84.13</b> ±0.35	<b>85.39</b> ±0.45	<b>90.98</b> ±0.29	<b>92.53</b> ±0.21	<b>93.26</b> ±0.24

**Zero-shot pathology detection.** Next, we investigate the unique ability of multimodal language modeling to leverage the language modality to perform ‘zero-shot’ classification. Without any explicit labels for downstream training, EEG may be classified by computing its similarity in latent space to text prompts representing the candidate classes. As suggested by [12], we create a prompt ensemble over 21 variations of the phrasing "The EEG is {normal, abnormal}" (Appendix C). Results in table 3 indicate that, despite a small dataset, EEG-language models can reach high levels of zero-shot pathology detection. The best models outperform all linear probes at 1% labels and even match EEG-only models at 100% labels. The clinical history, medication, and description models perform poorly, which follows from these models not being exposed to the explicit phrasing indicating the EEG status as normal or abnormal per se. Their performance can likely be improved by designing appropriate prompts.

Notably, while the ELM<sub>e,l</sub> models trained on either the interpretation cluster or all clusters both perform well with high consistency, training on LLM summaries resulted in highly variable scores. As the LLM-generated text was considerably more uniform with repetitive phrasing across reports, the lack of variability in combination with limited data may have led to unstable language representations of the text projector. Meanwhile, we observe the opposite pattern for ELM<sub>l</sub>, where LLM summaries enabled the only consistently above-chance zero-shot classifier. As with the report retrieval analysis, the fixed text representations of a language model which is not finetuned for EEG is likely inadequate to reliably separate between diverse descriptions of pathological and normal EEG. Meanwhile, the rigid LLM-generated text may have aided in this scenario by consistently yielding divergent text representations with which normal and abnormal EEG may be aligned. It must be noted that the current set-up may have favoured the LLM-generated summaries as they were used to subsample the dataset into a balanced subset. However, in this case it is likely this filtering step also aided other models by omitting some EEGs for which the pathology status was uncertain.

## 4 Discussion

The current work presents a first application of multimodal pretraining using natural language and functional brain data in a medical context. Our findings indicate that EEG-language pretraining provides better representations than EEG-only SSL. The richest representations appear to be obtained via a combination of contrastive learning and exposure to a variety of textual information. Specifically, combining information regarding the patient’s clinical history and medication as well as the physician’s description and interpretation of the EEG considerably improved retrieval performance. Such multimodal models were also found to be capable of zero-shot pathology detection. Using linear



Table 3: Pathology detection via zero-shot classification. The best scores are printed in bold. Standard deviation over five model training runs are included.

Method	Text Sampling	Balanced Accuracy	AUROC (%)	F1-Score (%)
ELM <sub>l</sub>	Clinical History	50.00±0.00	34.34±1.66	0.00±0.00
ELM <sub>l</sub>	Medication	50.00±0.00	74.99±1.80	0.00±0.00
ELM <sub>l</sub>	Description	50.00±0.00	43.70±1.99	0.00±0.00
ELM <sub>l</sub>	Interpretation	50.00±0.00	89.23±0.31	0.00±0.00
ELM <sub>l</sub>	LLM Summary	71.98±0.62	90.92±0.35	61.77±1.24
ELM <sub>l</sub>	All Clusters	50.00±0.00	84.52±0.57	0.00±0.00
ELM <sub>e,l</sub>	Clinical History	62.50±8.74	67.57±10.41	60.96±6.13
ELM <sub>e,l</sub>	Medication	51.09±17.79	52.21±23.54	50.67±12.53
ELM <sub>e,l</sub>	Description	64.03±3.95	71.40±4.32	63.56±3.81
ELM <sub>e,l</sub>	Interpretation	82.34±1.42	91.80±0.47	80.10±1.63
ELM <sub>e,l</sub>	LLM Summary	58.87±15.48	67.98±20.88	64.32±9.06
ELM <sub>e,l</sub>	All Clusters	<b>83.16</b> ±1.15	<b>91.91</b> ±0.67	<b>81.25</b> ±1.35

probing, sizable performance improvements over EEG-only SSL were observed, with the largest gains in contexts with few annotated samples.

Some considerations of the current study deserve mention. Due to clear data privacy concerns, no additional paired EEG-report datasets are publicly available, which currently prevents assessing the generalizability of our results across datasets. Although great care was taken to prevent data leakage and no model development involved any of the evaluation data, future work is required to properly study generalizability and scaling behavior as demonstrated in [22, 11]. While the retrieval analyses suggest that certain models learn richer data representations, a lack of annotations hindered a more detailed assessment of their utility for downstream tasks. Future research could benefit from annotations for specific pathologies, enabling more precise model comparisons. Additionally, we observed lower pathology detection scores for EEG-only SSL than a previous study [8], despite using the same data augmentations. Their work pretrained larger models on multiple datasets to output sequential representations. However, many such adaptations to the EEG encoder or its training could also be applied to EEG-language modeling. Finally, although several models displayed accurate zero-shot pathology detection, the variability in results may be due to the challenges of language modeling with limited data. Further research is needed to explore additional inductive biases or regularization of the text projector to address this issue.

## 5 Acknowledgments and Disclosure of Funding

This research was funded by the Deutsche Forschungsgemeinschaft (DFG) through FOR 5187 (project number 442075332). Additional support was provided by the DFG through the following projects: CRC 1404 (project number 414984028), TRR 265 (project number 402170461), and RU 5363 (project number 459422098).

The data used in this study was provided by the Neural Engineering Data Consortium at Temple University. For further details about this data, please access the following URL: [https://isip.piconepress.com/projects/tuh\\_eeg/html/downloads.shtml](https://isip.piconepress.com/projects/tuh_eeg/html/downloads.shtml).

The authors declare no competing interests.

## References

- [1] Colin D Binnie and Hermann Stefan. Modern electroencephalography: its role in epilepsy management. *Clinical Neurophysiology*, 110(10):1671–1697, 1999.
- [2] Jin Jing, Aline Herlopian, Ioannis Karakis, Marcus Ng, Jonathan J Halford, Alice Lam, Douglas Maus, Fonda Chan, Marjan Dolatshahi, Carlos F Muniz, et al. Interrater reliability of experts in identifying interictal epileptiform discharges in electroencephalograms. *JAMA neurology*, 77(1):49–57, 2020.
- [3] Raman K Malhotra and Alon Y Avidan. Sleep stages and scoring technique. *Atlas of sleep medicine*, pages 77–99, 2013.
- [4] Jared Kaplan, Sam McCandlish, Tom Henighan, Tom B Brown, Benjamin Chess, Rewon Child, Scott Gray, Alec Radford, Jeffrey Wu, and Dario Amodei. Scaling laws for neural language models. *arXiv preprint arXiv:2001.08361*, 2020.
- [5] Samuel L Smith, Andrew Brock, Leonard Berrada, and Soham De. Convnets match vision transformers at scale. *arXiv preprint arXiv:2310.16764*, 2023.
- [6] Raia Hadsell, Sumit Chopra, and Yann LeCun. Dimensionality reduction by learning an invariant mapping. In *2006 IEEE computer society conference on computer vision and pattern recognition (CVPR'06)*, volume 2, pages 1735–1742. IEEE, 2006.
- [7] Ting Chen, Simon Kornblith, Mohammad Norouzi, and Geoffrey Hinton. A simple framework for contrastive learning of visual representations. In *International conference on machine learning*, pages 1597–1607. PMLR, 2020.
- [8] Mostafa Neo Mohsenvand, Mohammad Rasool Izadi, and Pattie Maes. Contrastive representation learning for electroencephalogram classification. In *Machine Learning for Health*, pages 238–253. PMLR, 2020.
- [9] Chaoqi Yang, Danica Xiao, M Brandon Westover, and Jimeng Sun. Self-supervised eeg representation learning for automatic sleep staging. *arXiv preprint arXiv:2110.15278*, 2021.
- [10] Hubert Banville, Omar Chehab, Aapo Hyvärinen, Denis-Alexander Engemann, and Alexandre Gramfort. Uncovering the structure of clinical eeg signals with self-supervised learning. *Journal of Neural Engineering*, 18(4):046020, 2021.
- [11] Wei-Bang Jiang, Li-Ming Zhao, and Bao-Liang Lu<sup>12</sup>. Large brain model for learning generic representations with tremendous eeg data in bci. *ICLR*, 2024.
- [12] Alec Radford, Jong Wook Kim, Chris Hallacy, Aditya Ramesh, Gabriel Goh, Sandhini Agarwal, Girish Sastry, Amanda Askell, Pamela Mishkin, Jack Clark, et al. Learning transferable visual models from natural language supervision. In *International conference on machine learning*, pages 8748–8763. PMLR, 2021.
- [13] Yuhao Zhang, Hang Jiang, Yasuhide Miura, Christopher D Manning, and Curtis P Langlotz. Contrastive learning of medical visual representations from paired images and text. In *Machine Learning for Healthcare Conference*, pages 2–25. PMLR, 2022.
- [14] Sheng Zhang, Yanbo Xu, Naoto Usuyama, Hanwen Xu, Jaspreet Bagga, Robert Tinn, Sam Preston, Rajesh Rao, Mu Wei, Naveen Valluri, et al. Biomedclip: a multimodal biomedical foundation model pretrained from fifteen million scientific image-text pairs. *arXiv preprint arXiv:2303.00915*, 2023.
- [15] Iyad Obeid and Joseph Picone. The temple university hospital eeg data corpus. *Frontiers in neuroscience*, 10:195498, 2016.
- [16] Li Jing, Pascal Vincent, Yann LeCun, and Yuandong Tian. Understanding dimensional collapse in contrastive self-supervised learning. *arXiv preprint arXiv:2110.09348*, 2021.
- [17] Che Liu, Sibao Cheng, Chen Chen, Mengyun Qiao, Weitong Zhang, Anand Shah, Wenjia Bai, and Rossella Arcucci. M-flag: Medical vision-language pre-training with frozen language models and latent space geometry optimization. In *International Conference on Medical Image Computing and Computer-Assisted Intervention*, pages 637–647. Springer, 2023.
- [18] Zhi Zhang, Sheng-hua Zhong, and Yan Liu. Ganser: A self-supervised data augmentation framework for eeg-based emotion recognition. *IEEE Transactions on Affective Computing*, 2022.
- [19] Xingyi Wang, Yuliang Ma, Jared Cammon, Feng Fang, Yunyuan Gao, and Yingchun Zhang. Self-supervised eeg emotion recognition models based on cnn. *IEEE Transactions on Neural Systems and Rehabilitation Engineering*, 31:1952–1962, 2023.
- [20] Joseph Y Cheng, Hanlin Goh, Kaan Dogrusoz, Oncel Tuzel, and Erdrin Azemi. Subject-aware contrastive learning for biosignals. *arXiv preprint arXiv:2007.04871*, 2020.

- [21] Cédric Rommel, Joseph Paillard, Thomas Moreau, and Alexandre Gramfort. Data augmentation for learning predictive models on eeg: a systematic comparison. *Journal of Neural Engineering*, 19(6):066020, 2022.
- [22] Chaoqi Yang, M Westover, and Jimeng Sun. Biot: Biosignal transformer for cross-data learning in the wild. *Advances in Neural Information Processing Systems*, 36, 2024.
- [23] Subhrajit Roy, Isabell Kiral-Kornek, and Stefan Harrer. Chrononet: A deep recurrent neural network for abnormal eeg identification. In *Artificial Intelligence in Medicine: 17th Conference on Artificial Intelligence in Medicine, AIME 2019, Poznan, Poland, June 26–29, 2019, Proceedings 17*, pages 47–56. Springer, 2019.
- [24] Lukas AW Gemein, Robin T Schirrmeyer, Patryk Chrabaszcz, Daniel Wilson, Joschka Boedecker, Andreas Schulze-Bonhage, Frank Hutter, and Tonio Ball. Machine-learning-based diagnostics of eeg pathology. *NeuroImage*, 220:117021, 2020.
- [25] David Western, Timothy Weber, Rohan Kandasamy, Felix May, Samantha Taylor, Yixuan Zhu, and Luke Canham. Automatic report-based labelling of clinical eegs for classifier training. In *2021 IEEE Signal Processing in Medicine and Biology Symposium (SPMB)*, pages 1–6. IEEE, 2021.
- [26] Ann-Kathrin Kiessner, Robin T Schirrmeyer, Lukas AW Gemein, Joschka Boedecker, and Tonio Ball. An extended clinical eeg dataset with 15,300 automatically labelled recordings for pathology decoding. *NeuroImage: Clinical*, 39:103482, 2023.
- [27] Mohammad-Javad Darvishi-Bayazi, Mohammad Sajjad Ghaemi, Timothee Lesort, Md Rifat Arefin, Jocelyn Faubert, and Irina Rish. Amplifying pathological detection in eeg signaling pathways through cross-dataset transfer learning. *Computers in Biology and Medicine*, 169:107893, 2024.
- [28] Robin Tibor Schirrmeyer, Jost Tobias Springenberg, Lukas Dominique Josef Fiederer, Martin Glasstetter, Katharina Eggenberger, Michael Tangermann, Frank Hutter, Wolfram Burgard, and Tonio Ball. Deep learning with convolutional neural networks for eeg decoding and visualization. *Human brain mapping*, 38(11):5391–5420, 2017.
- [29] Fabien Lotte, Laurent Bougrain, Andrzej Cichocki, Maureen Clerc, Marco Congedo, Alain Rakotomamonjy, and Florian Yger. A review of classification algorithms for eeg-based brain–computer interfaces: a 10 year update. *Journal of neural engineering*, 15(3):031005, 2018.
- [30] Denis A Engemann, Federico Raimondo, Jean-Rémi King, Benjamin Rohaut, Gilles Louppe, Frédéric Faugeras, Jitka Annen, Helena Cassol, Olivia Gosseries, Diego Fernandez-Slezak, et al. Robust eeg-based cross-site and cross-protocol classification of states of consciousness. *Brain*, 141(11):3179–3192, 2018.
- [31] Shih-Cheng Huang, Liyue Shen, Matthew P Lungren, and Serena Yeung. Gloria: A multimodal global-local representation learning framework for label-efficient medical image recognition. In *Proceedings of the IEEE/CVF International Conference on Computer Vision*, pages 3942–3951, 2021.
- [32] Fuying Wang, Yuyin Zhou, Shujun Wang, Varut Vardhanabhuti, and Lequan Yu. Multi-granularity cross-modal alignment for generalized medical visual representation learning. *Advances in Neural Information Processing Systems*, 35:33536–33549, 2022.
- [33] Yinda Chen, Che Liu, Wei Huang, Sibó Cheng, Rossella Arcucci, and Zhiwei Xiong. Generative text-guided 3d vision-language pretraining for unified medical image segmentation. *arXiv preprint arXiv:2306.04811*, 2023.
- [34] Che Liu, Sibó Cheng, Miaoqing Shi, Anand Shah, Wenjia Bai, and Rossella Arcucci. Imitate: Clinical prior guided hierarchical vision-language pre-training. *arXiv preprint arXiv:2310.07355*, 2023.
- [35] Sravan Kumar Lalam, Hari Krishna Kunderu, Shayan Ghosh, Harish Kumar, Samir Awasthi, Ashim Prasad, Francisco Lopez-Jimenez, Zachi I Attia, Samuel Asirvatham, Paul Friedman, et al. Ecg representation learning with multi-modal ehr data. *Transactions on Machine Learning Research*, 2023.
- [36] Jun Li, Che Liu, Sibó Cheng, Rossella Arcucci, and Shenda Hong. Frozen language model helps ecg zero-shot learning. In *Medical Imaging with Deep Learning*, pages 402–415. PMLR, 2024.
- [37] Che Liu, Zhongwei Wan, Sibó Cheng, Mi Zhang, and Rossella Arcucci. Etp: Learning transferable ecg representations via ecg-text pre-training. In *ICASSP 2024-2024 IEEE International Conference on Acoustics, Speech and Signal Processing (ICASSP)*, pages 8230–8234. IEEE, 2024.
- [38] Che Liu, Zhongwei Wan, Cheng Ouyang, Anand Shah, Wenjia Bai, and Rossella Arcucci. Zero-shot ecg classification with multimodal learning and test-time clinical knowledge enhancement. *arXiv preprint arXiv:2403.06659*, 2024.
- [39] Qiao Jin, Won Kim, Qingyu Chen, Donald C Comeau, Lana Yeganova, W John Wilbur, and Zhiyong Lu. Medcpt: Contrastive pre-trained transformers with large-scale pubmed search logs for zero-shot biomedical information retrieval. *Bioinformatics*, 39(11):btad651, 2023.

- [40] Yu Gu, Robert Tinn, Hao Cheng, Michael Lucas, Naoto Usuyama, Xiaodong Liu, Tristan Naumann, Jianfeng Gao, and Hoifung Poon. Domain-specific language model pretraining for biomedical natural language processing. *ACM Transactions on Computing for Healthcare (HEALTH)*, 3(1):1–23, 2021.
- [41] Jean-Bastien Grill, Florian Strub, Florent Alché, Corentin Tallec, Pierre Richemond, Elena Buchatskaya, Carl Doersch, Bernardo Avila Pires, Zhaohan Guo, Mohammad Gheshlaghi Azar, et al. Bootstrap your own latent—a new approach to self-supervised learning. *Advances in neural information processing systems*, 33:21271–21284, 2020.
- [42] Adrien Bardes, Jean Ponce, and Yann LeCun. Vicreg: Variance-invariance-covariance regularization for self-supervised learning. *arXiv preprint arXiv:2105.04906*, 2021.
- [43] Sebas Lopez, G Suarez, D Jungreis, I Obeid, and Joseph Picone. Automated identification of abnormal adult eegs. In *2015 IEEE signal processing in medicine and biology symposium (SPMB)*, pages 1–5. IEEE, 2015.
- [44] Meta AI. Llama 3. [https://github.com/meta-llama/llama3/blob/main/MODEL\\_CARD.md](https://github.com/meta-llama/llama3/blob/main/MODEL_CARD.md), 2024.
- [45] Alexandre Gramfort, Martin Luessi, Eric Larson, Denis A. Engemann, Daniel Strohmeier, Christian Brodbeck, Roman Goj, Mainak Jas, Teon Brooks, Lauri Parkkonen, and Matti S. Hämäläinen. MEG and EEG data analysis with MNE-Python. *Frontiers in Neuroscience*, 7(267):1–13, 2013.
- [46] Yidong Wang, Zhuohao Yu, Jindong Wang, Qiang Heng, Hao Chen, Wei Ye, Rui Xie, Xing Xie, and Shikun Zhang. Exploring vision-language models for imbalanced learning. *International Journal of Computer Vision*, 132(1):224–237, 2024.
- [47] Yang You, Igor Gitman, and Boris Ginsburg. Large batch training of convolutional networks. *arXiv preprint arXiv:1708.03888*, 2017.
- [48] Emily Alsentzer, John R Murphy, Willie Boag, Wei-Hung Weng, Di Jin, Tristan Naumann, and Matthew McDermott. Publicly available clinical bert embeddings. *arXiv preprint arXiv:1904.03323*, 2019.
- [49] Michael Gutmann and Aapo Hyvärinen. Noise-contrastive estimation: A new estimation principle for unnormalized statistical models. In *Proceedings of the thirteenth international conference on artificial intelligence and statistics*, pages 297–304. JMLR Workshop and Conference Proceedings, 2010.
- [50] L Veloso, J McHugh, E von Weltin, S Lopez, I Obeid, and J Picone. Big data resources for eegs: Enabling deep learning research. In *2017 IEEE Signal Processing in Medicine and Biology Symposium (SPMB)*, pages 1–3. IEEE, 2017.
- [51] F. Pedregosa, G. Varoquaux, A. Gramfort, V. Michel, B. Thirion, O. Grisel, M. Blondel, P. Prettenhofer, R. Weiss, V. Dubourg, J. Vanderplas, A. Passos, D. Cournapeau, M. Brucher, M. Perrot, and E. Duchesnay. Scikit-learn: Machine learning in Python. *Journal of Machine Learning Research*, 12:2825–2830, 2011.
- [52] Laurens Van der Maaten and Geoffrey Hinton. Visualizing data using t-sne. *Journal of machine learning research*, 9(11), 2008.

## A Training Details

In this section, we provide further detailed information of the model training. Unless stated otherwise, ablation and hyperparameter analyses were performed on a data subset consisting of 5000 and 500 EEG recordings divided into a training and test set respectively. To prevent data leakage, this data had no overlap with the patients used for evaluation of the main results.

### A.1 Optimization

All models are trained using the LARS optimizer [47] with a cosine decay learning rate schedule over 50 epochs, with a warm-up of 4 epochs. The base learning rate is set to 0.3 for EEG-only and 0.01 for EEG-language models, scaled with the batch size ( $\text{BaseLR} \times \text{BatchSize}/256$  [41]). We use a weight-decay parameter of  $1 \times 10^{-4}$ . Models were trained on either an Nvidia Geforce GTX 3090 or Tesla V100 GPU and require less than 24GB of memory. Training took approximately 9 hours for EEG-language modeling or 18 hours for EEG-only modeling due to data augmentations. We used CUDA v12.3 and PyTorch v1.12.1.

### A.2 EEG Encoder

We use a CNN architecture with a residual stream as the EEG encoder for all analyses (Figure 4). The model uses parallel convolutions, involving reflection padding and 1D-convolutions with kernel sizes  $\{4, 8, 16\}$  with 32 filters each. These outputs are concatenated, resulting in a 96 dimensional representation and 747K trainable parameters. We compare input lengths of EEG crops varying from 5 to 60 seconds. This presents a trade-off where longer crops result in a greater information content per crop, while reducing the total sample size. As EEG-only pretraining relies on data augmentations, this introduces an additional influence of crop length. Specifically, longer crop lengths likely make the pretraining task easier, as augmentations introduce relatively lesser distortion due to the greater information content. We therefore compare performance of different crop lengths for both EEG-language and EEG-only pretraining. As the EEG encoder progressively downsamples the signal, we adjust the pooling layers to the input length. These adjustments are shown in Table A.2. For EEG-language pretraining we evaluate zero-shot pathology detection, while for EEG-only pretraining we are required to compare the performance of a linear probe. Results are shown in Figure 5. Due to computational resources, we only compare crop lengths for BYOL and  $\text{ELM}_l$  as representations of EEG-only and EEG-language modeling. We observe that for EEG-only pretraining an intermediate crop-length of 20 seconds performs best, which matches the findings by [8]. Meanwhile, zero-shot pathology detection is found to be insensitive to crop lengths of at least 10 seconds, with 60 second crops scoring highest, while the shortest crop length consistently leads to unstable text representations and chance-level performance.

For the EEG projector, we use a linear layer with an output dimension of 512 followed by batch normalization, exponential linear units, and a final linear layer with output size 256.

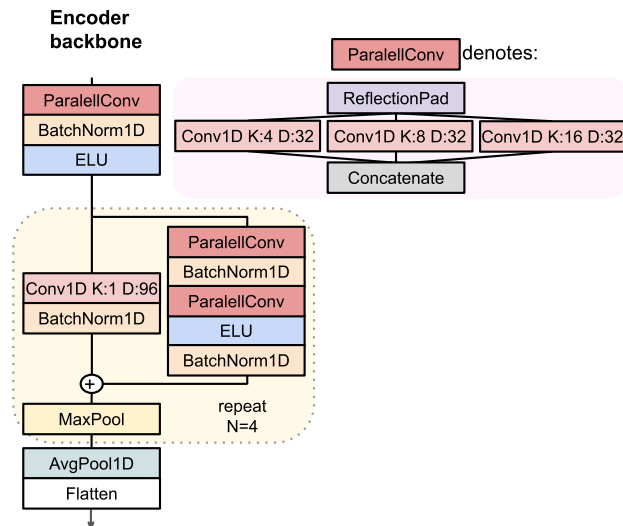


Figure 4: An identical EEG encoder architecture is used across all analyses. The size of the max pool operation depends on the input length. These are detailed in table A.2. K: Kernel size, D: Output dimensionality.

Table 4: Multiple input lengths for the cropped EEG timeseries were compared, which included adjustments to the pooling layer.

Model Setups			Batch Size	
Input Dim.	Max Pool Size	Intermediate Dim.	EEG+Text	EEG
500	[2,2,2,2]	[166, 55, 18, 6]	2048	2048
1000	[3,3,3,3]	[333, 111, 37, 12]	2048	2048
2000	[3,3,3,3]	[666, 222, 74, 24]	2048	1024
3000	[4,4,4,4]	[750, 187, 46, 11]	1024	800
6000	[4,4,4,4]	[1500, 375, 93, 23]	800	400

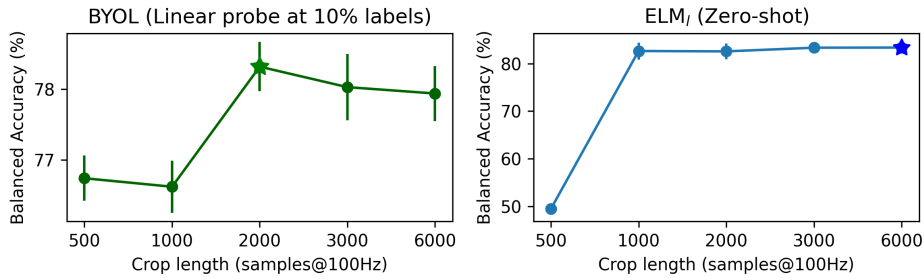


Figure 5: Comparison of pathology detection based on EEG input crop length, ranging from 5 to 60 seconds, via averaged balanced accuracy scores. Error bars indicate the standard deviation across five random seeds.

### A.3 Language Encoder

We compare three pretrained language models in their ability to perform zero-shot pathology detection following EEG-language pretraining (Table 5). We find that MedCPT performs best [39], which is trained using contrastive learning with 255 million user click logs from PubMed.

For the text projector of  $ELM_{e,l}$ , we use a linear layer with output size 1024 followed by batch normalization, rectified linear units, and a final linear layer with output size 256 and batch normalization.

Table 5: Zero-shot classification comparison between language models for  $ELM_{e,l}$ .

Language Model	Balanced Accuracy	AUROC
BiomedBERT [40]	78.61 $\pm$ 2.90	85.78 $\pm$ 2.58
Bio-ClinicalBERT [48]	80.86 $\pm$ 1.19	87.33 $\pm$ 0.68
MedCPT [39]	<b>82.58<math>\pm</math>0.25</b>	<b>88.37<math>\pm</math>0.39</b>

### A.4 Temperature parameter

For  $ELM_{e,l}$ , the softmax operation used in the loss computation includes a temperature hyperparameter  $\tau$ . We compare zero-shot pathology detection for multiple values. We observe poor performance for low temperature values, but stable zero-shot classification for higher parameter values. We set  $\tau = 0.3$  for all further analyses.

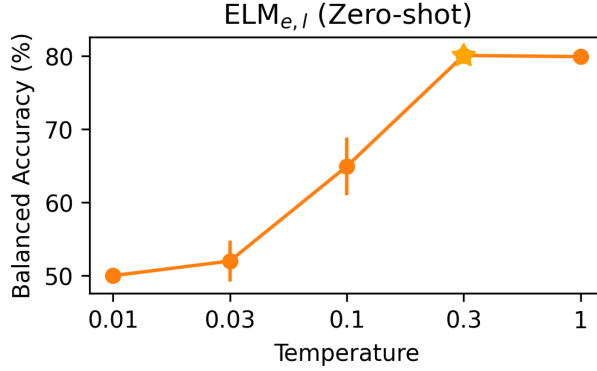


Figure 6: Comparison of temperature values for  $ELM_{e,l}$  on zero-shot pathology detection. Error bars indicate the standard deviation across three random seeds.

### A.5 EEG-Only Pretraining

We implement the following methods for EEG-only SSL:

**Bootstrap-Your-Own-Latent.** BYOL relies on two encoder models: an online and a target network [41]. During pretraining, the online network is trained to predict the target model’s output. Meanwhile, the weights of the target network are updated using a moving average of the weights of the online network, which has been empirically shown to prevent collapse of the latent space. For alignment,  $\ell_2$  normalization is applied to the EEG embeddings  $\{\mathbf{h}'_e, \mathbf{h}''_e\}$  and the mean square distance is minimized. We adopt the recommended parameter value for the exponential moving average [41]. The projection head is a 2-layer non-linear MLP with a hidden dimension of width 256 and an output dimension of 32.

**Variance-Invariance-Covariance Regularization.** VICReg allows for the use of a single encoder model and prevents collapse by applying two explicit regularization terms to each of the embedding batches  $\{\mathbf{h}'_e, \mathbf{h}''_e\}$  [42]. The ‘variance’ term maintains the standard deviation (computed batch-wise) of every embedding dimension above a threshold, thereby avoiding a trivial solution. In addition, latent collapse is avoided through the ‘covariance’ term which decorrelates pairs of embedding dimensions. The method minimizes the mean square distance between  $\{\mathbf{h}'_e, \mathbf{h}''_e\}$ . Hyperparameters are set to their recommended values [42]. The projection head is a 2-layer non-linear MLP with a hidden dimension of width 256 and an output dimension of 256.

**Contrast with the World Representation.** ContraWR was proposed to improve augmentation-based SSL for EEG [9]. The method, which is contrastive in nature, maximizes similarity between  $\{\mathbf{h}'_e, \mathbf{h}''_e\}$  while preventing collapse by minimizing similarity with ‘negative’ samples. ContraWR forms a negative representation by aggregating across all negative batch elements, aiming to compensate for the low signal-to-noise of EEG data by creating a more reliable negative contrast. It relies on a triplet loss based on Info-NCE [49]. We also here set the hyperparameters to the values recommended by the authors [9]. The projection head is a 2-layer non-linear MLP with a hidden dimension of width 256 and an output dimension of 32.

**Relative Positioning.** Pairs of EEG crops are sampled and assigned binary labels based on their temporal proximity [10]. Crops close in time are labeled positive, while those far apart are labeled negative. We use the same EEG encoder as for all other methods to create representations and use the suggested contrastive module to compute the element-wise absolute difference between representations. A logistic regression model then predicts the label. The method is trained using binary logistic loss. For all methods by [10], we use the hyperparameters reported to work best on TUAB, including between-subject sampling of EEG crops.

**Temporal Shuffling.** An extension of Relative Positioning by sampling triplets of EEG crops. The task is to determine whether the crops are in temporal order or shuffled [10]. The contrastive module concatenates absolute differences between representations. As with Relative Positioning, a logistic regression model is used for prediction, and the method is trained end-to-end using binary logistic loss.

**Contrastive Predictive Coding.** This method uses an autoregressive encoder to summarize a sequence of EEG crops into a context vector [10]. The task is to predict which future crop actually follows the context, among negative samples. A bilinear model is used for prediction at each future step. The method is trained end-to-end using the InfoNCE loss.

### A.5.1 Data augmentations

For EEG-only pretraining, we adapt the data augmentations proposed by Mohsenvand et al.[8], which were found to perform well on the TUAB dataset. For a given EEG crop, we apply the same augmentation to each channel. Parameters are sampled independently for each EEG crop and uniformly from the ranges displayed in table 6. Augmentations are visualized for a single EEG channel in figure 7.

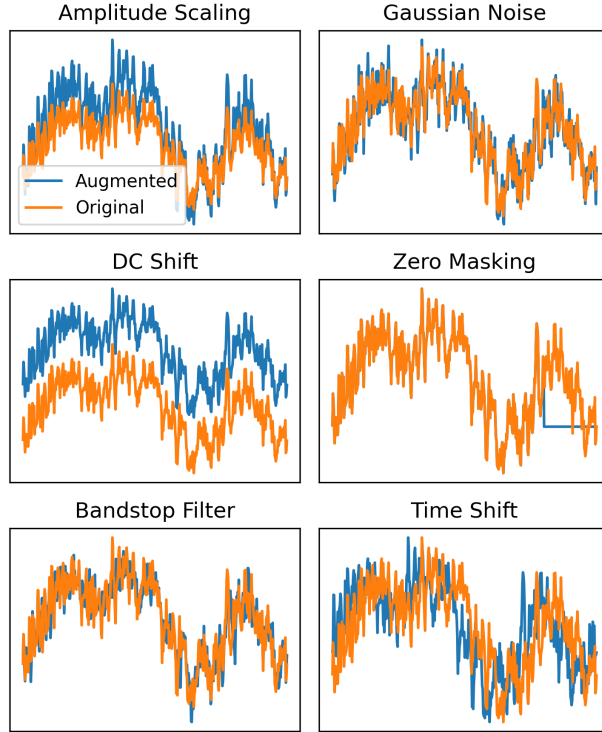


Figure 7: Data augmentations visualized for a single channel of EEG data.

Table 6: Data augmentation parameter ranges; adapted from [8].

Data Augmentation	Min	Max
Amplitude Scale	0.5	1.5
Time Shift in samples	-60	60
DC shift in microvolts	-10	10
Zero-Masking in samples	0	200
Additive Gaussian Noise (sigma)	0	0.2
Band-Stop Filter (5Hz width, Hz)	2.8	47

## B Details on Data Subsampling

To alleviate class imbalance in the TUEG dataset, we perform data subsampling. We rely on the LLM summaries of reports, which were more consistent in their phrasing regarding the normal or abnormal status. This allowed for a more reliable classification using regular expressions. All reports for which no clear classification was made were omitted. 5015 reports in the potential training set were classified as normal, which were associated with 7526 EEG recordings. For our ‘pretrain’ data subset, we subsampled the abnormal EEGs to match the amount of normal EEG recordings. This resulted in 7526 abnormal EEG recordings, with 6770 reports. Although only a minor subset of these preliminary classifications was manually verified, it is important to note that this process was solely to alleviate severe class imbalance and was not used for further analysis.



For EEG-language modeling, the pretrain subset was effectively smaller, as a report had to be omitted from pretraining when it did not contain at least one relevant heading. Out of the 15144 total EEG files, this resulted in pretrain sample sizes of: 14836 (clinical history cluster), 14320 (medication cluster), 14800 (description cluster), 14794 (interpretation cluster), and 14946 (all clusters).

To test for retrieval performance, we supplemented the TUAB test set with data from the TUH EEG Epilepsy Corpus [50] in an attempt to create a larger, roughly balanced evaluation set of those with and without pathology. For this, we only selected the first recording of a subject so that no multiple files from the same subject were present. Additionally, we only included reports which had at least one heading from each text cluster to allow for a fair comparison.

## C Classification

To study the predictive capability of learned representations after pretraining, we train linear probes and perform zero-shot classification.

### Linear probe

For linear evaluation, we train logistic linear regression models using 10-fold cross validation for each pretrained model using sklearn [51]. We perform grid-search over 45 logarithmically-spaced values for L2 regularization between  $10^{-6}$  and  $10^5$  via a validation set.

### Zero-shot classification

For zero-shot pathology detection, we perform an ensemble over 21 binary prompts, listed in Table 7. Prompt ensembling was shown to improve performance [12], but we employ it here also as the limited data is likely to lead to less stable representations, which may lead to sensitivity to phrasing. To inspect whether results are sensitive to changes to the prompt set, we perform a post-hoc analysis using the held-out test set that iteratively leaves one prompt out of the ensemble (Figure 8). We observe that results are consistent across such reduced prompt sets, except for the  $ELM_l$  model trained on the clinical history or interpretation clusters, although neither model reaches competitive performance. This set was only initially verified on the training set to enable model- and parameter-comparisons using zero-shot performance. Tuning is likely to enable further performance improvements, although the flexibility of the zero-shot approach may introduce severe risk of overfitting on the TUEG dataset.

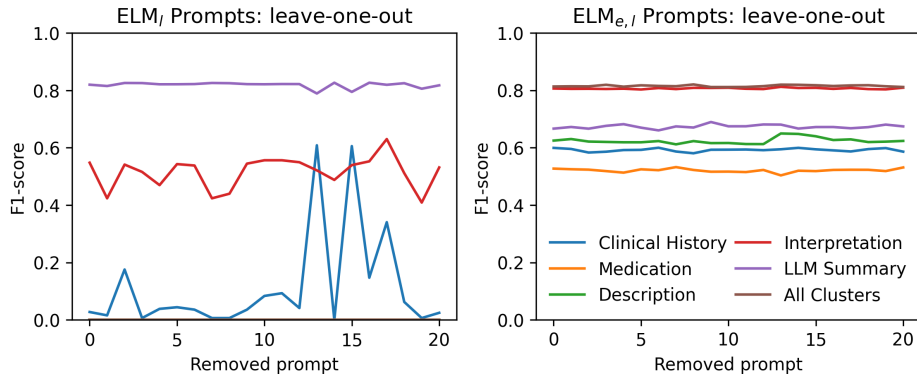


Figure 8: Analysis of the sensitivity to prompts in the ensemble used for zero-shot classification. We plot the average F1-score across five random seeds. Note that for  $ELM_l$ , multiple models have a consistent F1-score of 0 and are therefore not individually visible.

Table 7: Prompt ensemble used for zero-shot classification.

Normal EEG Prompts	Abnormal EEG Prompts
Normal EEG.	Abnormal EEG.
No pathology present.	Pathology present.
No abnormalities.	Abnormalities observed.
Normal routine EEG.	Markedly abnormal EEG.
Normal awake record.	Abnormal awake record.
Normal EEG record.	Abnormal EEG record.
This EEG is normal.	This EEG is abnormal.
This is a normal EEG.	This is an abnormal EEG.
This EEG is within normal limits	This EEG is mildly abnormal.
Normal awake EEG.	Abnormal awake EEG.
Normal asleep EEG.	Abnormal asleep EEG.
Normal awake and asleep EEG.	Abnormal awake and asleep EEG.
Normal EEG in wakefulness and drowsiness.	Abnormal EEG in wakefulness and drowsiness.
No pathology.	Abnormal EEG due to:
EEG shows no pathology.	Abnormal EEG for a subject of this age due to:
No abnormalities.	Abnormalities in the EEG.
No abnormalities observed.	Abnormalities observed.
EEG shows no abnormalities.	EEG shows abnormalities.
No clinical events detected.	Clinical events detected.
No indications of pathology observed.	Indications of pathology observed.
The EEG is normal.	The EEG is pathologically abnormal.

## D Post-hoc investigation of data leakage

To maximize the amount of data available in this data-scarce setting, the TUAB training set was included during pre-training. We investigate whether this gave a disproportionate advantage to linear probes trained on ELM representations by repeating the “1% labels” context using unseen subjects as follows: Given only the TUAB test set, we train linear probes using 10-fold cross validation (times five random seeds), each time splitting 10-20-70% of the test set into train/validation/test. This gives the same labeled sample size as 1% of the TUAB training set without relying on samples seen during pretraining. As seen in Table 8, results are highly similar, strongly suggesting that the advantage of ELMs is not due to the inclusion of the TUAB training set in the pretraining set.

Table 8: Effect of overlap in subjects used for pretraining and linear probing. Higher standard deviations result from a smaller test set.

Method	Overlap	Balanced Accuracy
TS	Yes	74.99 $\pm$ 0.86
TS	No	74.56 $\pm$ 1.12
ELM <sub>e,l</sub> All Clusters	Yes	82.64 $\pm$ 0.24
ELM <sub>e,l</sub> All Clusters	No	82.28 $\pm$ 0.64

## E Additional visualisations

### E.1 EEG embeddings

We provide t-SNE (complexity=40, [52]) visualisations of the averaged EEG embeddings per subject after pretraining. These are post-hoc plots for which we use models trained on the entire pretraining subset and display embeddings of hold-out TUAB patients. Multimodal modeling, specifically for ELM<sub>e,l</sub>, shows the clearest visual separation between abnormal and normal EEGs, which is in line with the linear probing results.

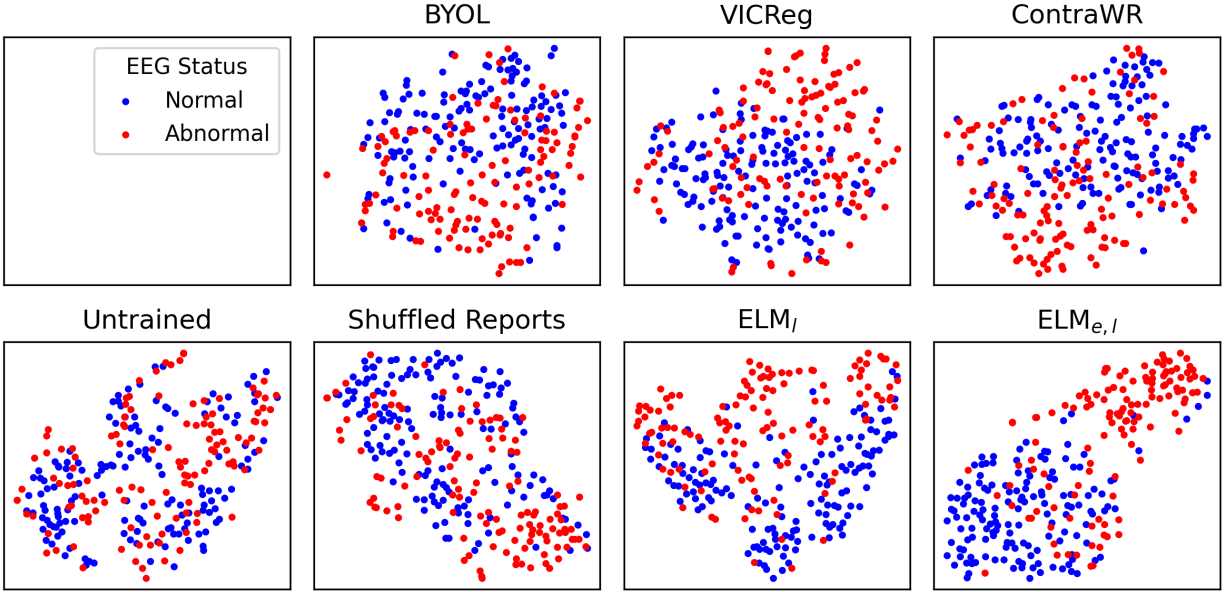


Figure 9: Example EEG embeddings averaged within-subject of pretrained models on the TUAB hold-out data. The data is projected using t-SNE. The ‘untrained’ and ‘shuffled reports’ plots feature the same setup as the  $ELM_{e,l}$  model, with the latter being trained on reports randomly shuffled between subjects.

E.2 Report and content segmentation

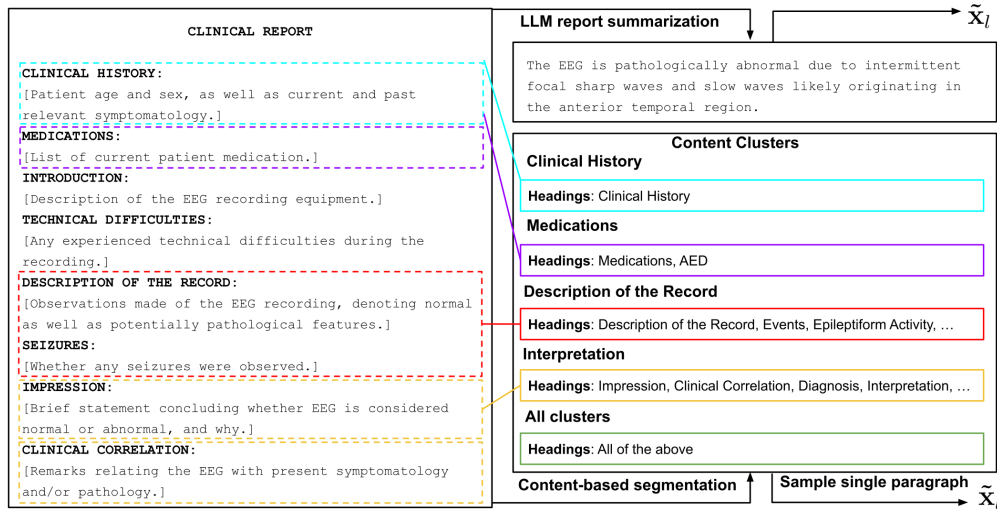


Figure 10: An example set of headings which may make up a clinical report. Paragraphs are extracted from the reports into content-based clusters or an LLM-generated summary.